Cerebral Cortex, April 2019;29: 1607–1618

doi: 10.1093/cercor/bhy059
Advance Access Publication Date: 28 March 2018
Original Article

ORIGINAL ARTICLE

Regional GABA Concentrations Modulate Inter-network Resting-state Functional Connectivity

Xi Chen[1,2], Xiaoying Fan[2], Yuzheng Hu[3], Chun Zuo[1], Susan Whitfield-Gabrieli[4], Daphne Holt[5], Qiyong Gong[6], Yihong Yang[3], Diego A. Pizzagalli[1,7], Fei Du[1,2] and Dost Ongur[2]

[1]McLean Imaging Center, McLean Hospital, Harvard Medical School, Belmont, MA 02478, USA, [2]Psychotic Disorders Division, McLean Hospital, Harvard Medical School, Belmont, MA 02478, USA, [3]Neuroimaging Research Branch, National Institute on Drug Abuse, Intramural Research Programs, National Institute of Health, Baltimore, MD 21224, USA, [4]McGovern Institute for Brain Research, Massachusetts Institute of Technology, Cambridge, MA 02139, USA, [5]Department of Psychiatry, Massachusetts General Hospital, Harvard Medical School, Charlestown, MA 02129, USA, [6]Huaxi MR Research Center (HMRRC), Department of Radiology, West China Hospital of Sichuan University, Chengdu, China and [7]Center For Depression, Anxiety and Stress Research, McLean Hospital, Harvard Medical School, Belmont, MA 02478, USA

Correspondence to: Fei Du, McLean Imaging Center, McLean Hospital, Harvard Medical School, Belmont, MA 02478, USA. Email: fdu@mclean.harvard.edu

Abstract

Coordinated activity within and differential activity between large-scale neuronal networks such as the default mode network (DMN) and the control network (CN) is a critical feature of brain organization. The CN usually exhibits activations in response to cognitive tasks while the DMN shows deactivations; in addition, activity between the two networks is anti-correlated at rest. To address this issue, we used functional MRI to measure whole-brain BOLD signal during resting-state and task-evoked conditions, and MR spectroscopy (MRS) to quantify GABA and glutamate concentrations, in nodes within the DMN and CN (MPFC and DLPFC, respectively) in 19 healthy individuals at 3 Tesla. We found that GABA concentrations in the MPFC were significantly associated with DMN deactivation during a working memory task and with anti-correlation between DMN and CN at rest and during task performance, while GABA concentrations in the DLPFC weakly modulated DMN–CN anti-correlation in the opposite direction. Highlighting specificity, glutamate played a less significant role related to brain activity. These findings indicate that GABA in the MPFC is potentially involved in orchestrating between-network brain activity at rest and during task performance.

Key words: anti-correlation, default mode network, fMRI, GABA, glutamate

Introduction

Coordinated activity across several large-scale neuronal networks subserves the complex and fluid functioning of the human brain. The default mode network (DMN) is characterized by increased activation during task-free resting period but becomes deactivated during externally oriented processing, which engages the frontoparietal executive control network (CN) (Buckner et al. 2008). Notably, DMN deactivation is proportional to external cognitive task load (Singh and Fawcett 2008; Hu et al. 2013), suggesting that a reallocation of cognitive

resources to goal-directed, attention-demanding tasks necessitates a suppression of the intrinsic brain activity in the DMN. In fact, better cognitive performance is associated with greater task-induced DMN deactivation (Anticevic et al. 2010). This phenomenon of coordinated activation–deactivation has been widely observed in task-related functional magnetic resonance imaging (fMRI) and resting-state fMRI (rsfMRI) studies. Failure to suppress DMN activity during tasks and reduced DMN–CN anti-correlation strength at rest has been observed in aging (Sambataro et al. 2010; Prakash et al. 2012) as well as neuropsychiatric disorders characterized by cognitive dysfunction, including Alzheimer's Disease, major depression, schizophrenia, and attention-deficit and hyperactivity disorder (Whitfield-Gabrieli et al. 2009; Chai et al. 2011; Anticevic et al. 2012; Baker et al. 2014). Despite the significance of system-level DMN–CN anti-correlation for brain function, the cellular and molecular mechanisms underlying this phenomenon are poorly understood.

DMN deactivation and DMN–CN anti-correlation have been associated with gamma oscillations (as assessed with electroencephalography, EEG) (Muthukumaraswamy et al. 2009), neurotransmitter concentrations (Northoff et al. 2007; Muthukumaraswamy et al. 2009; Hu et al. 2013), cerebral blood flow (Liang et al. 2013), and white matter fiber density (Hsu et al. 2016). Since rapid excitatory glutamate (Glu) and inhibitory γ-aminobutyric acid (GABA) signals mediate local and long-range neural circuits, studies relating Glu and GABA to cortical network function are particularly germane. Recent studies combining fMRI and magnetic resonance spectroscopy (MRS) have demonstrated that regional Glu and GABA concentrations are associated with their modulation of the BOLD signal in several important ways. For example, task-induced regional deactivation is negatively correlated with GABA concentration (Northoff et al. 2007; Hu et al. 2013) and positively correlated with Glu concentration (Enzi et al. 2012; Hu et al. 2013), and resting-state functional connectivity within DMN is associated with Glu and GABA concentrations in the posterior cingulate cortex/precuneus (PCC/PCu) (Kapogiannis et al. 2013). Thus, regional neurotransmitter concentrations modulate local task-related brain responses as well as resting-state functional connectivity.

Despite the importance of the topic for understanding brain function, no single study has systematically examined the relationship of GABA and Glu concentrations within the DMN and CN to resting-state anti-correlations and task-related activity in the human brain. Based on the known connectivity pattern of canonical cortical circuits, we hypothesized that glutamatergic and GABAergic measures would not only modulate local task-related activation–deactivation, but also correlate with DMN–CN anti-correlation measures at rest and during task performance (Fig. 1). However, the details of this hypothesis have not been tested. Specifically, is it inhibitory (GABA) or excitatory (Glu) signaling that drives the anti-correlation, and is it local (e.g., within DMN) or remote (e.g., between networks) signaling that matters? To address this fundamental issue, we collected resting-state functional connectivity (rsFC) data as well as fMRI during a working memory task intended to activate the CN and deactivate the DMN in a group of healthy individuals. In the same scan, we also measured the concentrations of GABA, Glu, and glutamine (Gln) at critical nodes within the DMN (medial prefrontal cortex (MPFC)) and CN (dorsolateral prefrontal cortex (DLPFC)). Finally, we probed the relationships between regional GABA and Glu concentrations within each network and the magnitude of DMN deactivation and DMN–CN anti-correlation at rest and during task performance.

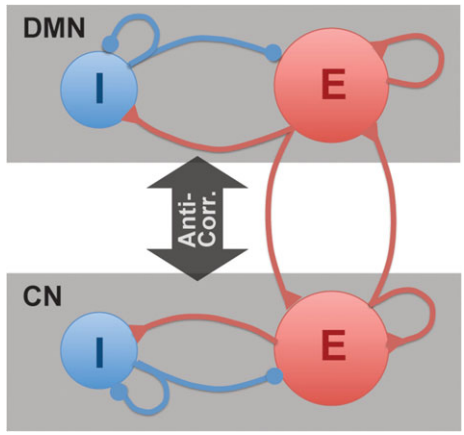

Figure 1. DMN–CN anti-correlation model with inhibitory (I) and excitatory (E) neurons. Rapid excitatory glutamate (Glu) and inhibitory γ-aminobutyric acid (GABA) signals mediate local and long-range neural circuits, including anti-correlation between DMN and CN. The local neurons project to remote network through excitatory transmitters.

Materials and Methods

Subjects

After giving informed consent, 19 healthy subjects (6 males, age range: 21–28 years; mean ± SD of age: 24 ± 2 years) participated in the study which was approved by the Partners Healthcare IRB. No subject had a history of medical, neurological, or psychiatric disorders, including current or past drug abuse and none were taking any medication.

MRS Data Acquisition and Processing

The following MRS and fMRI scans were performed on a Siemens 3 T Trio scanner using a 32-channel volume coil: a high-resolution anatomical scan (5 min), resting-state fMRI (6 min), followed by MRS (28 min for two locations), lastly, working memory (WM) fMRI (8 min). Single-voxel proton MRS was acquired at MPFC ($30 \times 20 \times 30\,mm^3$) and DLPFC ($25 \times 25 \times 35\,mm^3$) (Fig. 2c). A modified version of MEGA-PRESS (Rothman et al. 1984; Mescher et al. 1998) optimized in house (17) for GABA detection was acquired from both regions with the following parameters: TE/TR = 68/3000 ms and total 192 averages (scan time=10 min); the editing pulses applied alternatively at frequency of 1.9 or 7.5 ppm interleaved with the averages. A semi-LASER sequence (Scheenen et al. 2008; Oz and Tkac 2011) with optimized TE = 28 ms (Terpstra et al. 2016) and TR = 3 s and 64 averages (scan time = 4 min) was used to measure Glu and Gln from the same regions as MEGA-PRESS. Fastmap shimming (Gruetter 1993) was performed before MRS scans to ensure the full widths at half maxima (FWHM) of water resonance <12 Hz. A VAPOR (VAriable pulse Power and Optimized Relaxation delays) module (Tkac et al. 1999) was utilized in both sequences to achieve water suppression. Spectra with unsuppressed water were also acquired from the same VOI using the same MEGA-PRESS and semi-LASER sequences with nulling of the RF pulses of the water suppression module. The number of averages of the water spectra was 4. Water signal was used for eddy-current correction and as the external-reference for metabolite quantification. Spectra were saved individually and frequency and phase corrections processed in FID-A (Simpson et al. 2017). All MRS data were quantified using LCModel (version 6.3.1 H). Home-simulated basis spectra of

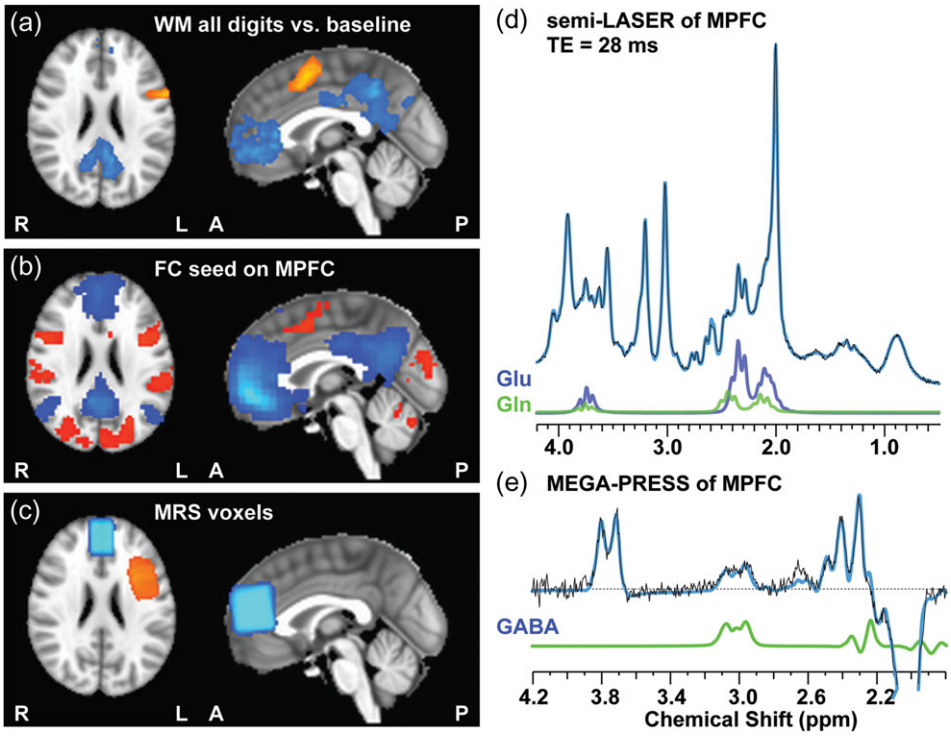

Figure 2. Group maps of working memory activations/deactivations (*a*), resting-state connectivity map with MPFC as seed (*b*), MRS voxels (*c*), and representative MR spectra of semi-LASER (*d*) and MEGA-PRESS (*e*) of MPFC.

Table 1 Information of ROIs obtained from WM 5d-1d activation/deactivation group map

ROI	MNI coordinates (mass center)	Cluster volumes (mm^3)	Brain regions	Brodmann area
MPFC	(−2.4, −45.4, −5.1)	7857	Medial Frontal Gyrus	10
DLPFC	(−44.9, 3.6, 34.7)	4239	Left Inferior Frontal Gyrus	9

metabolites were used in both MRS sequences with the addition of an experimental acquired macromolecule (MM) basis sets. The MRS signal is subject to different proton densities, T1 and T2 relaxation times in gray matter (GM), white matter (WM), and cerebrospinal fluid (CSF). Therefore, the volume fractions of different tissue types were calculated by segmenting T1 images in SPM12. Next, the water signal was corrected by tissue fractions with different proton density, T1 and T2 relaxations according to Table 1 of (Geramita et al. 2011). T1 and T2 values of GABA (T1 = 1310 ms, T2 = 88 ms) (Edden et al. 2012; Puts et al. 2013) and Glu (T1 = 1270 ms, T2 = 181ms) (Mlynarik et al. 2001; Ganji et al. 2012) were used for a global relaxation correction. It was assumed that there is no contribution to GABA and Glu MR signal from CSF. The proton density ratios of WM to GM (WM/GM) of GABA (0.67) (Geramita et al. 2011; Zhu et al. 2011) and Glu (0.5) (Choi et al. 2006; Srinivasan et al. 2006; Pan et al. 2010) were used to calculate the GABA and Glu concentrations in GM. Gln concentration was calculated using the same assumptions as those in the calculation of Glu concentration. The equation (Geramita et al. 2011) for correction calculations is outlined as follows:

$$(S_{met}/S_{wat})_{corr} = (S_{met}/S_{wat})_{uncorr} \cdot \frac{\left(WM\% \cdot f_{wat\_WM} + GM\% \cdot f_{wat\_GM} + CSF\% \cdot f_{wat\_csf}\right)}{\left(WM\% \cdot f_{met\_WM} + GM\% \cdot f_{met\_GM}\right)}$$

where S is the metabolite/water signal; WM%, GM% and CSF% are the tissue percentages; *f* is the sensitivity factor of metabolite/water in a certain tissue type.

Working Memory Task

The WM task used is a variation of the Sternberg item recognition paradigm (Sternberg 1966), a continuous performance, choice reaction time-task adapted for fMRI. It requires participants to first encode a set of digits (encode-phase) and then to maintain them "on-line" in WM while responding to each of the probe digits that follow by indicating whether or not it was a member of the memorized set (probe-phase). In our study, the Sternberg WM task design is similar to previous report (Kim et al. 2009). Each block began with a learn prompt that lasted for 2 s and displayed the word "Learn," then an encoding epoch with the presentation of a memory set composed of one, three, or five digits (1d, 3d or 5d) contributing to 3 levels WM load for 6 s, followed by a 38 s recognition epoch with the presentation of 14 probe digits. For each probe participants were presented with a single digit for 1.1 s, where half the digits are targets and the other half are foils. Delay between each probe digit was randomized around 1.6 s. Two blocks of 3 loads, totally 6 working memory blocks with pseudorandom order, were interleaved

by fixation baseline (fixation cross on the screen) with random duration between 4 and 20 s. All subjects went through the exact same Sternberg task sequence during imaging after practicing a brief version of the task outside the scanner.

fMRI Data Collection

Resting and WM task BOLD fMRI data were collected using a single-shot gradient-echo echo-planar imaging sequence. The imaging parameters were: TR/TE = 2500/30 ms; FA = 78°; slice thickness/gap = 4/0 mm; 39 slices; FOV = 220 × 220 mm^2 (3.44 × 3.44 mm^2 in-plane resolution). The anatomical data were acquired for structural reference using a T1-weighted 3D magnetization prepared rapid gradient echo (MP-RAGE) sequence (256 × 256 × 122 matrix size; 1 × 1 × 1.28 mm^3 spatial resolution; TI/TR/TE = 1100/1600/2.25 ms; flip angle = 12°).

Data Preprocessing and Analysis of Working Memory fMRI

All preprocessing and statistical analysis of WM fMRI were conducted with FSL 5.0 (FMRIB). The first two volumes were removed to allow for signal to reach a steady state. Preprocessing included motion correction (MCFLIRT), spatial smoothing using a 5 mm FWHM Gaussian kernel, 4D grand mean scaling, high-pass temporal filtering with a cutoff period of 100 s and pre-whitening using FILM. Non-brain structures were stripped from functional and anatomical volumes using FSL's Brain Extraction Tool. Smoothed functional data were normalized into MNI space of 3 × 3 × 3 mm^3 via high-resolution anatomic imaging using FSL's non-linear registration tool FNRT.

First level brain activation at 1d, 3d, and 5d conditions were estimated with AFNI 3dDeconvolve using general linear modeling. A box function convoluted with hemodynamic response function was used to create regressors for each condition. Group level analyses on the brain activation at 3 conditions were carried out using AFNI 3dttest++. The multiple comparison correction was performed with the 3dClustSim simulation of the newest version of AFNI (version 17.3.09, Dec. 2017), i.e., the 3dttest++ was used to generate 10 000 noise volumes by using the residuals of actual data sets with randomized signs, and 3dClustSim was used to perform the simulation. In this method, no built-in math model for the spatial auto-correlation function was used in order to better control false positive rate (Eklund et al. 2016). According to the simulation result (see Supplemental Table S1), fMRI activation/deactivation regions of interest (ROIs) of MPFC and DLPFC were determined by the criteria of voxel-wise $P < 0.001$ and cluster size >150 voxels, corresponding to corrected P value < 0.01. Individual mean BOLD signal beta values were extracted from these R01s as a quantification of the DMN deactivation and CN activation.

Data Preprocessing and Analysis of Resting-state/Working Memory Connectivity

Preprocessing of the rsfMRI data was carried out in DPARSFA (Yan and Zang 2010) and included removing first 5 time points, slice-timing correction, realignment, head motion correction, Gaussian spatial smoothing (FWHM = 4 mm), linear detrending, and spatial normalization to MNI space with a resampling resolution of 3 × 3 × 3 mm^3. Nuisance signal regressions and band-pass temporal filtering (passband: 0.01–0.1 Hz) were also performed. The nuisance regressors included Friston's 24 head motion parameters (6 head motion parameters, 6 head motion parameters one time point before, and the 12 corresponding squared items) (Friston et al. 1996) and 5 principal components of principal time courses extracted from respective white matter and cerebral spinal fluid (CSF) fluctuations using the anatomical CompCor (aCompCor) method (Behzadi et al. 2007). To minimize the influence of head motion in the rsFC analysis, data points when the instantaneous head motion, defined by framewise displacement (FD) (Power et al. 2012) was larger than 0.5 mm, as well as the one time points before and after "bad" time points were used as regressors in the nuisance regression. To further validate the findings, a more stringent cutoff (i.e., FD < 0.25 mm) was used and relative results are demonstrated in the Supplementary Materials. The residual is equivalent to performing censored regression only within the "good" data without motion contamination, since the strong signal outliers present during periods of motion thus likely corrupted the fits of nuisance regressors to data (Carp 2013; Power et al. 2013). Subjects with mean FD > 0.3 mm were excluded from analysis. The above mentioned MPFC ROI obtained from the WM activation/deactivation map was also used as the seed region in the FC analysis to identify the brain regions functionally connected to MPFC. Specifically, individual rsFC maps were generated by correlating the rsfMRI time course of each voxel with the mean reference time course of the seed MPFC region and then converting the correlation value to z value via Fisher's r-to-z transformation. The previously mentioned DLPFC ROI obtained from the WM activation/deactivation map was used to extracted functional connectivity between MPFC and DLPFC. The data processing of correlation of BOLD signal time series with working memory task follows exactly same strategy as that of rsFC. Last, an alternative process with global signal regressions (GSR) was also performed to demonstrate the strength of the reported findings. The results from this analysis are presented in the Supplementary Materials.

Statistics Analysis

Linear multiple-regression analysis was performed in IBM SPSS Statistics Version 24. Gender and MRS-measured GABA and Glu from MPFC or DLPFC were included as independent variables to predict fMRI measures. A multiple regression model including gender and rsFC between MPFC and DLPFC was also used to predict the MPFC–DLPFC anti-correlation during WM task. The age of 19 healthy subjects was within a very small range (21–28 years) and standard deviation (2 years) so it was not included as a coefficient in the model. We calculated the metabolite concentrations in gray matter with the information of tissue percentages and the prior knowledge of metabolite WM/GM concentration ratios, therefore GM percentage of the MRS voxel was not included in the analysis.

We included gender in our statistical model because gender effects have been reported on GABA concentration measures (O'Gorman et al. 2011; Aufhaus et al. 2013). Gray matter percentage was also included as a coefficient in the multiple regression analysis (Hu et al. 2013), especially when the metabolite differences between gray matter and white matter were not accounted for. The proton density ratios of WM to GM (WM/GM) of GABA (0.67) (Geramita et al. 2011; Zhu et al. 2011) and Glu (0.5) (Choi et al. 2006; Srinivasan et al. 2006; Pan et al. 2010) were confirmed by several independent studies. Also the relation between GM percentage and measured metabolite concentrations is non-linear and therefore not appropriate to be included in the linear regression model. Thus, instead of including MRS voxel GM% as a coefficient in multiple-regression analysis,

we calculated the metabolite concentrations in MPFC and DLPFC in pure gray matter with the information of tissue percentages and the prior knowledge of metabolite WM/GM concentration ratios.

Results

Functional MRI

Group maps of working memory activations/deactivations, resting-state functional connectivity with MPFC as seed are shown in Table 1 and Figure 2*a* and *b*, respectively. One subject with average FD > 0.3 mm in resting-state fMRI was excluded. DMN deactivation and CN activation can be clearly observed in the group map of WM fMRI, as well as the anti-correlation between DMN and CN in the group map of rsFC. The deactivation/activation signals at different WM task loads (1d, 3d, and 5d) were quantitatively demonstrated in Figure 3*a*. It is interesting to observe that when task load increased from low to medium level (1d to 3d) CN nodes showed enhanced activation but when task load increased to the highest level (5d), both CN node activation and DMN node deactivation were seen.

Magnetic Resonance Spectroscopy

The group map of the MPFC and DLPFC MRS voxels are presented in Figure 2*c*. Representative MR spectra obtained using semi-LASER and MEGA-PRESS from MPFC are shown in Figure 2*d* and *e*, respectively. FWHM of NAA resonance using MEGA-PRESS were 4.7 ± 1.0 Hz and 5.0 ± 0.8 Hz and using semi-LASER are 3.4 ± 1.2 Hz and 3.7 ± 0.7 Hz in the MPFC and DLPFC, respectively. Cramer-Rao lower bounds (CRLBs) of GABA using MEGA-PRESS were 6 ± 2% and 6 ± 1% and CRLBs of Gln/Glu using semi-LASER were 10 ± 2%/2.8 ± 0.4% and 1.6 ± 4%/3.2 ± 0.4% in the MPFC and DLPFC respectively. The values of correlation coefficient (cc) between Glu and Gln outputted from LCModel

Table 2 Regressing MPFC contrast of different WM loads on gender and neurotransmitters

WM load contrast	R^2	Adjusted R^2	P	Gender		GABA		Glu	
				Beta[a]	P	Beta[a]	P	Beta[a]	P
5d-1d	0.438	0.318	0.040	−0.530	0.032	−0.678	0.012	0.231	0.327
5d-3d	0.316	0.170	0.139	−0.437	0.096	−0.586	0.041	0.055	0.830
3d-1d	0.234	0.070	0.276	−0.224	0.401	−0.424	0.147	0.431	0.127

[a]Standardized coefficient.

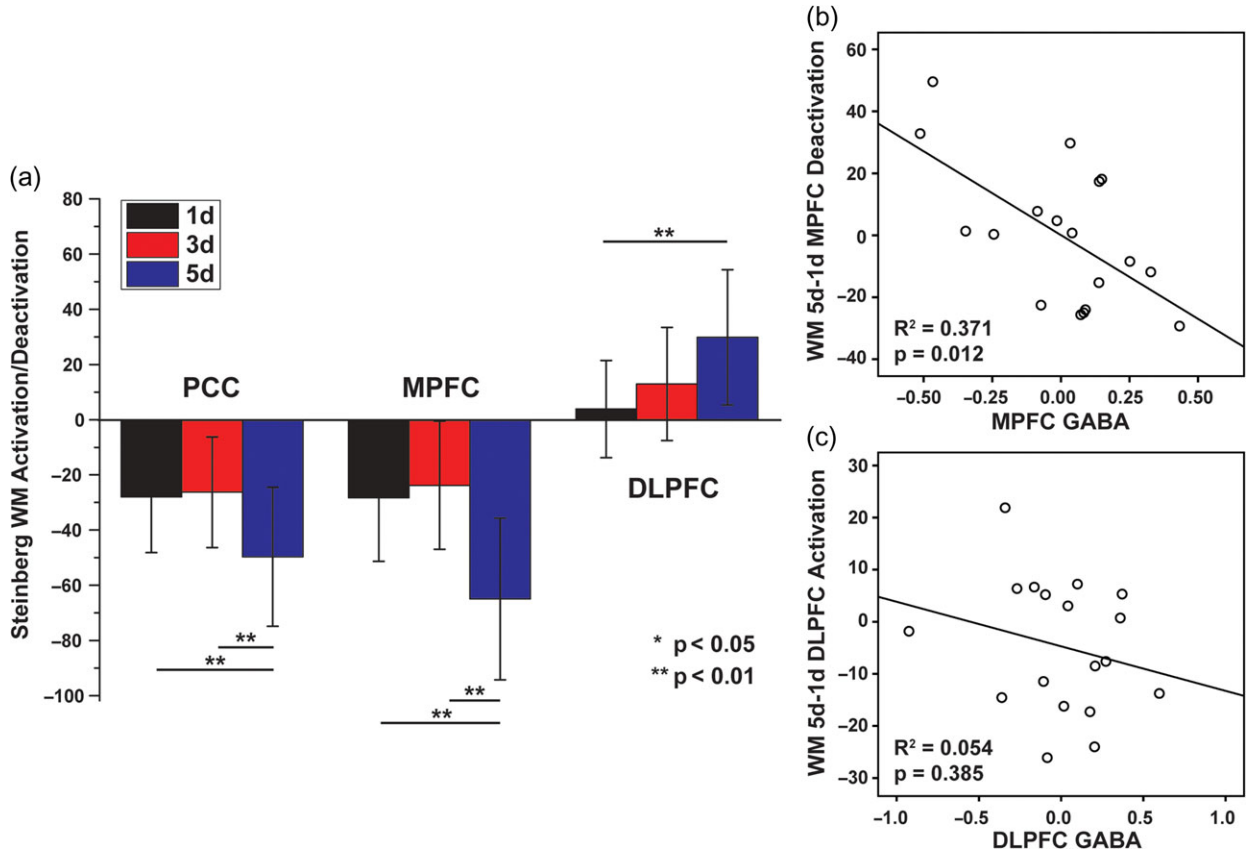

Figure 3. (*a*) In Steinberg WM task, cognitive load (1d, 3d and 5d) modulated activation/deactivation in the PCC/MPFC/DLPFC/ACC regions. Partial plots of the relationship between (*b*) WM deactivation in MPFC and MPFC GABA concentrations and (*c*) WM activation in DLPFC and DLPFC GABA concentrations, controlling gender and regional Glu concentrations.

were 0.08 ± 0.06 and 0.10 ± 0.07 in MPFC and DLPFC, respectively. All these measures indicate high MRS data quality acquired at our 3 T clinical scanner. No subject was excluded based on CRLBs or linewidth criteria.

Modulation of WM Activation/Deactivation by Regional Neurotransmitters

A multiple regression analysis was performed to regress MPFC deactivation of the contrast of different loads (5d-1d, 3d-1d, 5d-3d, respectively) on gender and partial volume effect corrected GABA and Glu in the same region (Table 2). The MPFC BOLD signal contrast between 5d and 1d showed strong dependence on GABA concentration of the same region (Fig. 3*b*) in that the higher individual GABA concentration in DMN predicted stronger DMN deactivation. On the other hand, the multiple regression analysis showed that the MRS measured Glu concentration played a less significant role in the interaction with DMN deactivation. A weaker relationship with regional neurotransmitters was also observed in the two smaller task load contrasts (5d-3d, 3d-1d). In contrast to the MPFC findings, GABA or Glu concentrations in the DLPFC had no relationship with activation in the DLPFC. In addition, GABA and Glu concentrations in the MPFC were unrelated to WM-evoked brain activations in DLPFC, and GABA and Glu concentrations in the DLPFC were unrelated to WM-evoked deactivations in MPFC.

Modulation of Resting-state DMN–CN Anti-correlation by Regional Neurotransmitters

A multiple regression analysis was performed to regress resting-state MPFC–DLPFC FC on gender and partial volume effect corrected GABA and Glu. There are two models: (I) with MPFC GABA/Glu and (II) with DLPFC GABA/Glu (Table 3) as regressors, respectively. Model I shows strong dependence of resting-state MPFC–DLPFC FC on MPFC neurotransmitters: more MPFC GABA predicte stronger anti-correlation between MPFC and DLPFC, while MPFC Glu weakly affected the anti-correlation in the opposite direction (Fig. 4). Neurotransmitter concentrations in the DLPFC showed no relationship to DMN–CN anti-correlation.

Modulation of DMN–CN Anti-correlation During WM task by Resting-state Anti-correlation and Regional Neurotransmitters

Unlike in the resting-state where fluctuations are spontaneously occurring, the DMN and CN are actively modulated in opposite directions during performance of a WM task (Anticevic et al. 2010). Using the same MPFC ROI, we found that the group time courses during the WM task showed stronger MPFC–DLPFC anti-correlation (adj $R^2 = 0.24$, $P = 8.83e{-}10$) compared to resting-state (adj $R^2 = 0.14$, $P = 4.89e{-}6$). We performed a multiple regression analysis to regress MPFC–DLPFC FC on 3 models: (I) gender and resting-state MPFC–DLPFC FC, (II) gender and partial volume effect corrected GABA/Glu in MPFC, and (III) gender and partial volume effect corrected GABA/Glu in DLPFC (Table 4). The results show that Model I with resting-state FC had the strongest predicting power for WM FC (Fig. 5*a*). Compared to the relation between resting-state anti-correlation and MPFC GABA/Glu, Model II showed weaker relation of WM anti-correlation with both MPFC GABA and Glu, while the correlation with MPFC GABA remained significant and preserved the same trend as at rest: higher MPFC GABA predicted stronger WM anti-correlation (Fig. 5*b*). Model III did not reveal any significant relationships (Fig. 5*c*).

Glutamine Relates to Brain Activity

Gln is synthesized from Glu by Gln synthethase in the astroglia and it is broken down to Glu by phosphate-activated glutaminase in neurons. Because of its role in the Glu–Gln neurotransmitter cycling and in glutamatergic synaptic function, we replaced Glu by Gln in the above analyses but no significant findings emerged.

Discussion

In this study, we collected whole-brain resting-state and task-evoked fMRI data as well as MRS data, at first time probing GABA and Glu concentrations in nodes of MPFC and DLPFC how to modulate anti-correlation between DMN and CN. Our findings indicate that GABA concentrations (related to inhibitory neurotransmission) – but not Glu concentration – is involved in orchestrating between-network interactions. In addition, there we found a unidirectional influence in between-network interactions, where neurotransmitter content in the MPFC (a node in the DMN) was critical but that in the DLPFC (a node in the CN) was not.

Neurotransmitters and Brain Functional Activity

The BOLD signal is an indirect measure of brain activity. It cannot provide insights into the mechanisms behind behavioral responses nor assess changes in excitatory/inhibitory (E/I) balance. In this context, our study provides new insights into how network interactions are orchestrated in the brain. First, our finding of a negative correlation between GABA concentrations and DMN deactivation agrees with its profile as the major post-synaptic inhibitory neurotransmitter. This relationship between GABA and BOLD signal is highly concordant across different studies from the visual cortex (Muthukumaraswamy et al. 2009, 2012; Donahue et al. 2010; Qin et al. 2012), auditory (Gao et al. 2015), sensorimotor (Stagg et al. 2011; Hayes et al. 2013) and anterior cingulate cortex (Northoff et al. 2007; Wiebking, Duncan, Qin et al. 2014). Our result is also consistent with a previous study of the PCC/PCu region of the DMN, using an n-back WM task strategy (Hu et al. 2013; Wiebking, Duncan, Qin et al. 2014).

Table 3 Regressing resting-state MPFC–DLPFC FC on gender and neurotransmitters

Models	R^2	Adjusted R^2	P	Gender		GABA		Glu	
				Beta[a]	P	Beta[a]	P	Beta[a]	P
I: MPFC GABA/Glu	0.761	0.710	0.000	0.160	0.408	−0.661	0.001	0.329	0.059
II: DLPFC GABA/Glu	0.389	0.258	0.068	0.345	0.126	0.409	0.101	0.132	0.576

[a]Standardized coefficient.

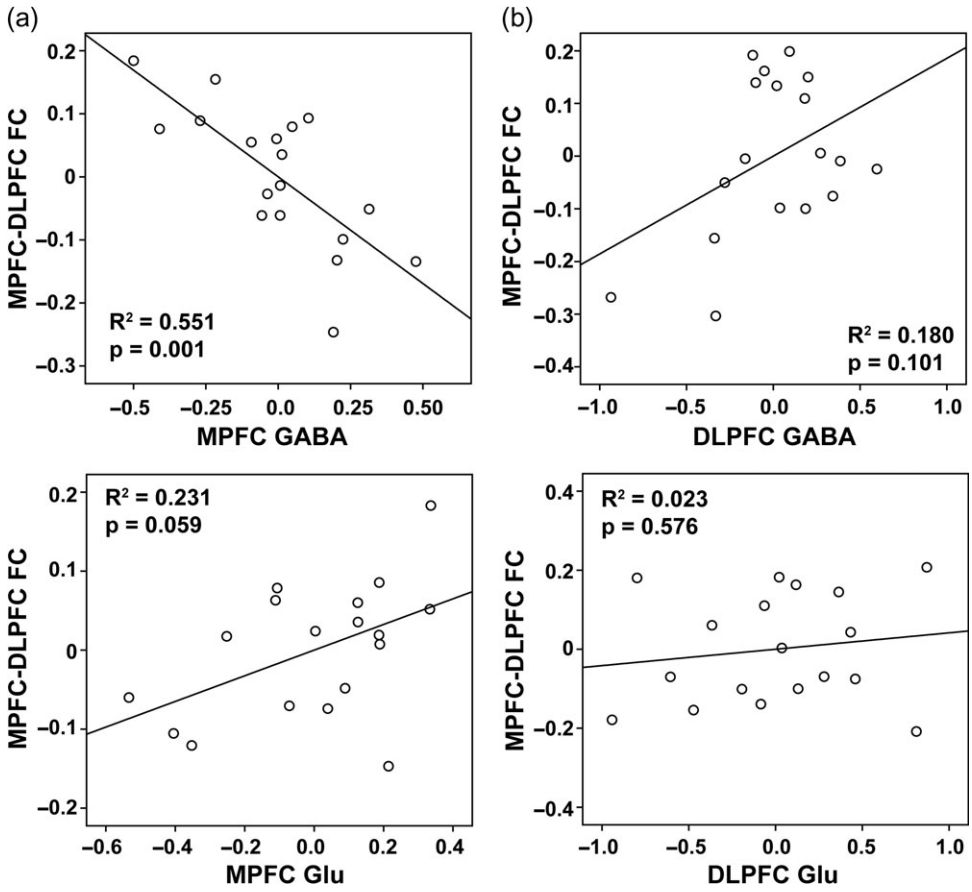

Figure 4. Partial plots of the relationship between MPFC–DLPFC resting-state FC and (*a*) MPFC GABA/Glu and (*b*) DLPFC GABA/Glu concentrations, controlling gender effect.

Table 4 Regressing MPFC–DLPFC FC during WM task on gender and rsFC/neurotransmitters

Models	R^2	Adjusted R^2	*P*	Coefficient 1			Coefficient 2			Coefficient 3		
				Name	Beta[a]	*P*	Name	Beta[a]	*P*	Name	Beta[a]	*P*
I: MPFC–DLPFC rsFC	0.673	0.629	0.000	Gender	−0.248	0.143	rsFC	0.884	0.000			
II: MPFC GABA/Glu	0.430	0.307	0.044	Gender	−0.181	0.432	GABA	−0.729	0.008	Glu	0.058	0.804
III: DLPFC GABA/Glu	0.048	−0.156	0.869	Gender	−0.003	0.992	GABA	0.184	0.532	Glu	−0.210	0.480

[a]Standardized coefficient.

A PET-fMRI study also confirmed the MPFC GABAA receptor binding observed by PET negatively correlates with BOLD signal change in the same area when performing an external awareness task (Wiebking, Duncan, Qin et al. 2014). In addition to modulating local BOLD responses, we show that higher MPFC GABA concentrations are associated with stronger MPFC–DLPFC anti-correlation at rest and during a WM task. During the WM task, GABA in DMN and CN may reach a new balance to achieve the task-mode anti-correlations, which could explain the reduced coupling between resting-state GABA and the anti-correlations during task.

Consistent with the literature (Northoff et al. 2007; Muthukumaraswamy et al. 2009, 2012; Donahue et al. 2010; Qin et al. 2012; Duncan et al. 2014; Wiebking, Duncan, Qin et al. 2014), our results also indicate that compared to GABA, Glu plays a less significant role in modulating local neuronal response to external stimulations and orchestration of between-network activity. Anti-correlation between networks, by definition, must involve inhibition; thus, the inhibitory effect of GABA on excitatory neurons and their remote projections may influence anti-correlations (Fig. 1). Compared to the moderate relationship between MPFC GABA and WM anti-correlation, the much stronger couplings of MPFC GABA with rsFC and rsFC with WM FC implies that the modulation on WM anti-correlation by MPFC GABA may not be a direct relationship and could be mediated by resting-state anti-correlation. Using functional MRS to observe neurotransmitter concentration changes during a WM task may provide further information of the modulation of anti-correlation during task.

In this study, we focused on the interaction between DMN and CN. Nodes within each network are anatomically connected to one another but the anatomical connections between these networks (e.g., between the DLPFC and MPFC) are not strong (Carmichael and Price 1996). This raises the question of

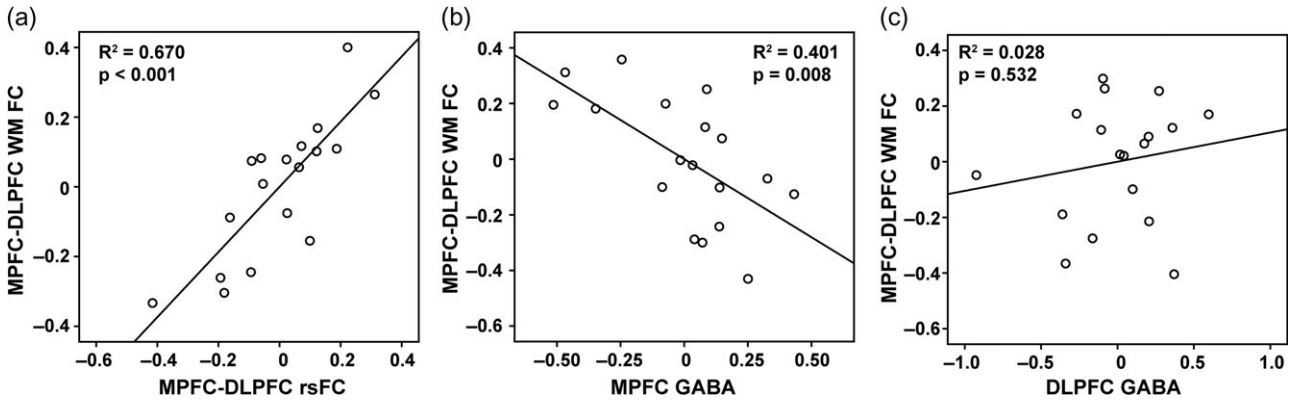

Figure 5. Partial plots of the relationship between MPFC–DLPFC FC during WM task and (a) MPFC–DLPFC resting-state FC, (b) MPFC GABA and (c) DLPFC GABA concentrations, controlling gender effect (a, b and c) and Glu concentrations in the same region (b and c).

how the anti-correlations between brain networks are orchestrated. The answer likely involves interactions with third brain regions as well as lateral inhibition through the anatomical connections that do exist. This need further study.

Understanding E/I Balance in Brain Networks Associated with Brain Disorders

Recent studies indicate that the specific behavioral and physiological measures (for example, impulsivity and sensorimotor response time) in participants are related to individual differences in regional GABA or Glu levels (Boy et al. 2010; Fusar-Poli et al. 2011; Wiebking, Duncan, Qin et al. 2014). The prefrontal cortex plays a key role in cognition and reward processing through its regulation of limbic reward regions and its involvement in higher-order executive function (Kalivas et al. 2005; Goldstein and Volkow 2011). Although it is poorly understood how neurophysiological substrates and neurochemicals modulate cognition and behavior for most psychiatric diseases and substance use disorders (SUD), one emerging principle is that there is a balance and coordinated activity between excitatory glutamatergic and inhibitory GABAergic neurons. The imbalance of cortical cellular excitation and inhibition could give rise to the abnormalities observed in SZ or SUD (Yizhar et al. 2011; Jocham et al. 2012; Cocchi et al. 2013; Gipson et al. 2013). One popular hypothesized mechanism for decision-making is competition via mutual inhibition, during which each available option inhibits others until activity remains in only one (Yizhar et al. 2011; Jocham et al. 2012; Cocchi et al. 2013). The neural dynamics of value comparison depend on the levels of Glu and GABA (D'Souza and Markou 2013; Li et al. 2014; Wiebking, Duncan, Qin et al. 2014; Wiebking, Duncan, Tiret et al. 2014) through increased activity in excitatory neurons or reduced in inhibitory neurons. Accumulating evidence also suggests that blockage of glutamatergic or facilitation of GABAergic transmission would inhibit the reward-enhancing and conditioned rewarding effects (Kalivas 2009; Gipson et al. 2013; Li et al. 2014). There is a report of a positive correlation between magnitude of MPFC–DLPFC anti-correlation and WM capacity for young adults (Hampson et al. 2010), as well as findings of reduced MPFC–DLPFC resting-state anti-correlation and reduced WM capacity in schizophrenia patients (Whitfield-Gabrieli et al. 2009) and older healthy subjects (Keller et al. 2015). Therefore, we chose the MPFC and DLPFC as the targeted voxels to measure GABA and Glu, and explored how E/I balance modulates local neuronal response to stimulus and brain networks. Our results indicate that inhibitory neurotransmission is actively modulated and provides the differential signal for changing E/I balance in brain circuits implicated in psychiatric disorders such as schizophrenia.

Limitations

Technically, the GABA measurement is challenging: it is subject to low SNR, motion artifact, and MM co-editing. The degree of MM signal contamination varies with sequences and parameters (Henry et al. 2001; Terpstra et al. 2002; Near et al. 2011). The symmetric editing method (Henry et al. 2001) can suppress the co-edited MM signal but a recent study shows that the MM-suppressed GABA signal is very sensitive to frequency drift (Edden et al. 2016). On the other hand, previous studies (Hofmann et al. 2001; Mader et al. 2002) suggested that the MM concentrations in cortical regions of healthy adults are very stable with respect to age and gender. Therefore, individual differences in the contaminated GABA levels may reflect primarily the differences in GABA itself. Compared to the regular PRESS method, the adiabatic pulse train of our semi-LASER sequence not only minimizes the voxel displacement caused by chemical shifts, but also obtains longer apparent T2 relaxation times of metabolites (Michaeli et al. 2002). Furthermore, J-evolution is partially suppressed in semi-LASER and observation of J-coupled metabolites such as glutamate and glutamine is favored (Oz and Tkac 2011). Short TE ^{1}H-MRS can achieve more reliable Glu detections. However, quantification of Gln is more challenging at 3 T due to severe overlapping with stronger Glu signal. In our current study, CRLBs of Glu and Gln and cc values of Glu and Gln indicate good separation of these metabolites. However, using ^{1}H-MRS to detect synaptic Glu is an unsolved issue. The ^{1}H MRS signal arises from all "free" Glu and not only those at the synapse. It cannot distinguish the Glu packed in synaptic vesicles (20–30% of total) from the metabolic pool in cytosol (~50%) (Nedergaard et al. 2002). Glu found in the synaptic cleft (~100 umol/L) is below the detection limit of ^{1}H MRS. On the other hand, Glu is rapidly converted to its metabolite Gln by the glia-specific enzyme glutamine synthetase in glial cells (Popoli et al. 2012). Accumulating evidence suggests that the Gln/Glu ratio may be somewhat more specific as a synaptic measure because it reflects the relative amounts of metabolite in neurons and astrocytes, respectively (Rowland et al. 2005; Xu et al. 2005; Chowdhury et al. 2011). Therefore, we also analyzed the relation between neurotransmitters and functional MRI measures by replacing the coefficient of

Glu by Gln/Glu ratio. The trends in the multiple-regression models remained unchanged in this approach. Notably, other factors such as the Gln–Glu cycling rate also affect the relationship between Gln/Glu ratio and synaptic Glu. As a result, the limitation of ^{1}H MRS compromises the detection of Glu synaptic release, which could represent one of the reasons why our regression models testing excitatory neurotransmitters showed a much weaker role than GABA. Lastly, in our study, the neurotransmitters in MPFC measured in resting state have a stronger relation with the anti-correlation during resting state than working memory task. It would be interesting to assess change in neurotransmitter levels during task and how they relate to brain activity (Huang et al. 2015; Kuhn et al. 2016; Ip et al. 2017). However, the limited sensitivity at 3 T prevents us from carrying out such an fMRS study. Use of an ultra-high field scanner such as 7 T with advanced MRS approaches could help address this issue as well as allow us to collect MRS data from the whole brain.

Motion correction is an important issue for functional connectivity data processing (Power et al. 2012, 2014, 2015, 2017; Satterthwaite et al. 2012; Burgess et al. 2016; Siegel et al. 2017). In this paper we performed nuisance regressions including Friston's 24 head motion parameters and 5 principal components of principal time courses extracted from respective white matter and cerebral spinal fluid (CSF) fluctuations using the anatomical CompCor (aCompCor) method (Behzadi et al. 2007), as well as the "bad" time point scrubbing regressors with criteria of FD = 0.5 mm (Power et al. 2012, 2013) and 0.25 mm (Yan et al. 2013; Power et al. 2014). Global signal regression (GSR) was also conducted to explore the impact of GSR on our findings. Both analyses (thresholding with FD = 0.25 mm and GSR, see Supplementary Materials) show similar findings to those reported above. Using FD = 0.25 mm led to the removal of more than 40 time points (almost 1/3 of total) for 3 subjects. Future studies using shorter TR and longer acquisition times (e.g., multiband fMRI) can address this concern and retain more valid data in the analyses.

The impact of including GSR in data analyses, especially when it comes to inter-regional anti-correlations, is controversial (Murphy et al. 2009; Saad et al. 2012). Nevertheless, in our study the functional connectivities processed either with or without GSR showed significant associations with MPFC GABA concentrations and not with DLPFC GABA concentrations.

Summary

We found that MPFC GABA concentrations significantly modulated DMN deactivation during a WM task, as well as the anti-correlation between DMN and ECN during both resting state and WM task. On the other hand, DLPFC GABA concentrations did not show significant associations in the above functional MRI measures. These findings suggest that MPFC and DLPFC GABA activity make differential impacts on task-related activation and inter-network functional connectivity. Exploring neurochemical characteristics of DMN and CN may provide novel insights into abnormal brain network activity and provide opportunities for developing novel treatment strategies and earlier interventions for neuropsychiatric disorders (Fox et al. 2014; Drysdale et al. 2017).

Supplementary Material

Supplementary material is available at *Cerebral Cortex* online.

Funding

This work was partially supported by grants from NARSAD (F.D.), MH114020 (FD), MH094594 (D.O.), MH104449 (D.O.). Y.H. and Y.Y. are supported by the Intramural Research Program of the National Institute on Drug Abuse of the National Institutes of Health. Over the past 3 years, Dr Pizzagalli has received consulting fees from Akili Interactive Labs, BlackThorn Therapeutics, Boehringer Ingelheim, Pfizer and PositScience for activities unrelated to the current research. Dr Ongur served on an Advisory Board for Neurocrine Inc. in 2017. All other authors report no biomedical financial interests.

Notes

The authors thank Drs Dinesh Deelchand (UMN), Gulin Oz (UMN), Malgorzata Marjanska (UMN), and Edward J. Auerbach (UMN and Siemens) for their assistance in the experiments and thoughtful discussions. *Conflict of Interest*: None declared.

References

Anticevic A, Cole MW, Murray JD, Corlett PR, Wang XJ, Krystal JH. 2012. The role of default network deactivation in cognition and disease. Trends Cogn Sci. 16:584–592.

Anticevic A, Repovs G, Shulman GL, Barch DM. 2010. When less is more: TPJ and default network deactivation during encoding predicts working memory performance. NeuroImage. 49: 2638–2648.

Aufhaus E, Weber-Fahr W, Sack M, Tunc-Skarka N, Oberthuer G, Hoerst M, Meyer-Lindenberg A, Boettcher U, Ende G. 2013. Absence of changes in GABA concentrations with age and gender in the human anterior cingulate cortex: a MEGA-PRESS study with symmetric editing pulse frequencies for macromolecule suppression. Magn Reson Med. 69:317–320.

Baker JT, Holmes AJ, Masters GA, Yeo BT, Krienen F, Buckner RL, Ongur D. 2014. Disruption of cortical association networks in schizophrenia and psychotic bipolar disorder. JAMA Psychiatry. 71:109–118.

Behzadi Y, Restom K, Liau J, Liu TT. 2007. A component based noise correction method (CompCor) for BOLD and perfusion based fMRI. NeuroImage. 37:90–101.

Boy F, Evans CJ, Edden RA, Singh KD, Husain M, Sumner P. 2010. Individual differences in subconscious motor control predicted by GABA concentration in SMA. Curr Biol. 20: 1779–1785.

Buckner RL, Andrews-Hanna JR, Schacter DL. 2008. The brain's default network: anatomy, function, and relevance to disease. Ann N Y Acad Sci. 1124:1–38.

Burgess GC, Kandala S, Nolan D, Laumann TO, Power JD, Adeyemo B, Harms MP, Petersen SE, Barch DM. 2016. Evaluation of denoising strategies to address motion-correlated artifacts in resting-state functional magnetic resonance imaging data from the human Connectome Project. Brain Connect. 6:669–680.

Carmichael ST, Price JL. 1996. Connectional networks within the orbital and medial prefrontal cortex of macaque monkeys. J Comp Neurol. 371:179–207.

Carp J. 2013. Optimizing the order of operations for movement scrubbing: comment on Power et al. NeuroImage. 76: 436–438.

Chai XJ, Whitfield-Gabrieli S, Shinn AK, Gabrieli JD, Nieto Castanon A, McCarthy JM, Cohen BM, Ongur D. 2011.

Abnormal medial prefrontal cortex resting-state connectivity in bipolar disorder and schizophrenia. Neuropsychopharmacology. 36:2009–2017.

Choi C, Coupland NJ, Bhardwaj PP, Kalra S, Casault CA, Reid K, Allen PS. 2006. T2 measurement and quantification of glutamate in human brain in vivo. Magn Reson Med. 56:971–977.

Chowdhury GM, Behar KL, Cho W, Thomas MA, Rothman DL, Sanacora G. 2011. 1)H-[(13)C]-nuclear magnetic resonance spectroscopy measures of ketamine's effect on amino acid neurotransmitter metabolism. Biol Psychiatry. 71(11): 1022–1025.

Cocchi L, Zalesky A, Fornito A, Mattingley JB. 2013. Dynamic cooperation and competition between brain systems during cognitive control. Trends Cogn Sci. 17:493–501.

Donahue MJ, Near J, Blicher JU, Jezzard P. 2010. Baseline GABA concentration and fMRI response. NeuroImage. 53:392–398.

Drysdale AT, Grosenick L, Downar J, Dunlop K, Mansouri F, Meng Y, Fetcho RN, Zebley B, Oathes DJ, Etkin A, et al. 2017. Resting-state connectivity biomarkers define neurophysiological subtypes of depression. Nat Med. 23:28–38.

Duncan NW, Wiebking C, Northoff G. 2014. Associations of regional GABA and glutamate with intrinsic and extrinsic neural activity in humans – a review of multimodal imaging studies. Neurosci Biobehav Rev. 47:36–52.

D'Souza MS, Markou A. 2013. The "stop" and "go" of nicotine dependence: role of GABA and glutamate. Cold Spring Harb Perspect Med. 3(6):a012146.

Edden RA, Intrapiromkul J, Zhu H, Cheng Y, Barker PB. 2012. Measuring T2 in vivo with J-difference editing: application to GABA at 3 Tesla. J Magn Reson Imaging. 35:229–234.

Edden RA, Oeltzschner G, Harris AD, Puts NA, Chan KL, Boer VO, Schar M, Barker PB. 2016. Prospective frequency correction for macromolecule-suppressed GABA editing at 3T. J Magn Reson Imaging. 44:1474–1482.

Eklund A, Nichols TE, Knutsson H. 2016. Cluster failure: Why fMRI inferences for spatial extent have inflated false-positive rates. Proc Natl Acad Sci. 113:7900–7905.

Enzi B, Duncan NW, Kaufmann J, Tempelmann C, Wiebking C, Northoff G. 2012. Glutamate modulates resting state activity in the perigenual anterior cingulate cortex – a combined fMRI-MRS study. Neuroscience. 227:102–109.

Fox MD, Buckner RL, Liu H, Chakravarty MM, Lozano AM, Pascual-Leone A. 2014. Resting-state networks link invasive and noninvasive brain stimulation across diverse psychiatric and neurological diseases. Proc Natl Acad Sci USA. 111: E4367–E4375.

Friston KJ, Williams S, Howard R, Frackowiak RS, Turner R. 1996. Movement-related effects in fMRI time-series. Magn Reson Med. 35:346–355.

Fusar-Poli P, Stone JM, Broome MR, Valli I, Mechelli A, McLean MA, Lythgoe DJ, O'Gorman RL, Barker GJ, McGuire PK. 2011. Thalamic glutamate levels as a predictor of cortical response during executive functioning in subjects at high risk for psychosis. Arch Gen Psychiatry. 68:881–890.

Ganji SK, Banerjee A, Patel AM, Zhao YD, Dimitrov IE, Browning JD, Brown ES, Maher EA, Choi C. 2012. T2 measurement of J-coupled metabolites in the human brain at 3T. NMR Biomed. 25:523–529.

Gao F, Wang G, Ma W, Ren F, Li M, Dong Y, Liu C, Liu B, Bai X, Zhao B, et al. 2015. Decreased auditory GABA+ concentrations in presbycusis demonstrated by edited magnetic resonance spectroscopy. NeuroImage. 106:311–316.

Geramita M, van der Veen JW, Barnett AS, Savostyanova AA, Shen J, Weinberger DR, Marenco S. 2011. Reproducibility of prefrontal gamma-aminobutyric acid measurements with J-edited spectroscopy. NMR Biomed. 24:1089–1098.

Gipson CD, Reissner KJ, Kupchik YM, Smith AC, Stankeviciute N, Hensley-Simon ME, Kalivas PW. 2013. Reinstatement of nicotine seeking is mediated by glutamatergic plasticity. Proc Natl Acad Sci USA. 110:9124–9129.

Goldstein RZ, Volkow ND. 2011. Dysfunction of the prefrontal cortex in addiction: neuroimaging findings and clinical implications. Nat Rev Neurosci. 12:652–669.

Gruetter R. 1993. Automatic, localized in vivo adjustment of all first- and second-order shim coils. Magn Reson Med. 29: 804–811.

Hampson M, Driesen N, Roth JK, Gore JC, Constable RT. 2010. Functional connectivity between task-positive and task-negative brain areas and its relation to working memory performance. Magn Reson Imaging. 28:1051–1057.

Hayes DJ, Duncan NW, Wiebking C, Pietruska K, Qin P, Lang S, Gagnon J, Bing PG, Verhaeghe J, Kostikov AP, et al. 2013. GABAA receptors predict aversion-related brain responses: an fMRI-PET investigation in healthy humans. Neuropsychopharmacology. 38:1438–1450.

Henry PG, Dautry C, Hantraye P, Bloch G. 2001. Brain GABA editing without macromolecule contamination. Magnet Reson Med. 45:517–520.

Hofmann L, Slotboom J, Boesch C, Kreis R. 2001. Characterization of the macromolecule baseline in localized (1)H-MR spectra of human brain. Magn Reson Med. 46:855–863.

Hsu LM, Liang X, Gu H, Brynildsen JK, Stark JA, Ash JA, Lin CP, Lu H, Rapp PR, Stein EA, et al. 2016. Constituents and functional implications of the rat default mode network. Proc Natl Acad Sci USA. 113:E4541–E4547.

Hu Y, Chen X, Gu H, Yang Y. 2013. Resting-state glutamate and GABA concentrations predict task-induced deactivation in the default mode network. J Neuroscience. 33:18566–18573.

Huang Z, Davis HH IV, Yue Q, Wiebking C, Duncan NW, Zhang J, Wagner NF, Wolff A, Northoff G. 2015. Increase in glutamate/glutamine concentration in the medial prefrontal cortex during mental imagery: a combined functional mrs and fMRI study. Hum Brain Mapp. 36:3204–3212.

Ip IB, Berrington A, Hess AT, Parker AJ, Emir UE, Bridge H. 2017. Combined fMRI-MRS acquires simultaneous glutamate and BOLD-fMRI signals in the human brain. NeuroImage. 155: 113–119.

Jocham G, Hunt LT, Near J, Behrens TE. 2012. A mechanism for value-guided choice based on the excitation-inhibition balance in prefrontal cortex. Nat Neurosci. 15:960–961.

Kalivas PW. 2009. The glutamate homeostasis hypothesis of addiction. Nat Rev Neurosci. 10:561–572.

Kalivas PW, Volkow N, Seamans J. 2005. Unmanageable motivation in addiction: a pathology in prefrontal-accumbens glutamate transmission. Neuron. 45:647–650.

Kapogiannis D, Reiter DA, Willette AA, Mattson MP. 2013. Posteromedial cortex glutamate and GABA predict intrinsic functional connectivity of the default mode network. NeuroImage. 64:112–119.

Keller JB, Hedden T, Thompson TW, Anteraper SA, Gabrieli JD, Whitfield-Gabrieli S. 2015. Resting-state anticorrelations between medial and lateral prefrontal cortex: association with working memory, aging, and individual differences. Cortex. 64:271–280.

Kim DI, Manoach DS, Mathalon DH, Turner JA, Mannell M, Brown GG, Ford JM, Gollub RL, White T, Wible C, et al. 2009. Dysregulation of working memory and default-mode networks in schizophrenia using independent component

analysis, an fBIRN and MCIC study. Hum Brain Mapp. 30: 3795–3811.

Kuhn S, Schubert F, Mekle R, Wenger E, Ittermann B, Lindenberger U, Gallinat J. 2016. Neurotransmitter changes during interference task in anterior cingulate cortex: evidence from fMRI-guided functional MRS at 3 T. Brain Struct Funct. 221:2541–2551.

Li X, Semenova S, D'Souza MS, Stoker AK, Markou A. 2014. Involvement of glutamatergic and GABAergic systems in nicotine dependence: Implications for novel pharmacotherapies for smoking cessation. Neuropharmacology. 76 (Pt B):554–565.

Liang X, Zou Q, He Y, Yang Y. 2013. Coupling of functional connectivity and regional cerebral blood flow reveals a physiological basis for network hubs of the human brain. Proc Natl Acad Sci USA. 110:1929–1934.

Mader I, Seeger U, Karitzky J, Erb M, Schick F, Klose U. 2002. Proton magnetic resonance spectroscopy with metabolite nulling reveals regional differences of macromolecules in normal human brain. J Magn Reson Imaging. 16:538–546.

Mescher M, Merkle H, Kirsch J, Garwood M, Gruetter R. 1998. Simultaneous in vivo spectral editing and water suppression. NMR Biomed. 11:266–272.

Michaeli S, Garwood M, Zhu XH, DelaBarre L, Andersen P, Adriany G, Merkle H, Ugurbil K, Chen W. 2002. Proton T2 relaxation study of water, N-acetylaspartate, and creatine in human brain using Hahn and Carr-Purcell spin echoes at 4T and 7T. Magn Reson Med. 47:629–633.

Mlynarik V, Gruber S, Moser E. 2001. Proton T (1) and T (2) relaxation times of human brain metabolites at 3 Tesla. NMR Biomed. 14:325–331.

Murphy K, Birn RM, Handwerker DA, Jones TB, Bandettini PA. 2009. The impact of global signal regression on resting state correlations: are anti-correlated networks introduced? NeuroImage. 44:893–905.

Muthukumaraswamy SD, Edden RA, Jones DK, Swettenham JB, Singh KD. 2009. Resting GABA concentration predicts peak gamma frequency and fMRI amplitude in response to visual stimulation in humans. Proc Natl Acad Sci USA. 106: 8356–8361.

Muthukumaraswamy SD, Evans CJ, Edden RA, Wise RG, Singh KD. 2012. Individual variability in the shape and amplitude of the BOLD-HRF correlates with endogenous GABAergic inhibition. Hum Brain Mapp. 33:455–465.

Near J, Simpson R, Cowen P, Jezzard P. 2011. Efficient gamma-aminobutyric acid editing at 3T without macromolecule contamination: MEGA-SPECIAL. NMR Biomed. 24:1277–1285.

Nedergaard M, Takano T, Hansen AJ. 2002. Beyond the role of glutamate as a neurotransmitter. Nat Rev Neurosci. 3:748–755.

Northoff G, Walter M, Schulte RF, Beck J, Dydak U, Henning A, Boeker H, Grimm S, Boesiger P. 2007. GABA concentrations in the human anterior cingulate cortex predict negative BOLD responses in fMRI. Nat Neurosci. 10:1515–1517.

Oz G, Tkac I. 2011. Short-echo, single-shot, full-intensity proton magnetic resonance spectroscopy for neurochemical profiling at 4 T: validation in the cerebellum and brainstem. Magn Reson Med. 65:901–910.

O'Gorman RL, Michels L, Edden RA, Murdoch JB, Martin E. 2011. In vivo detection of GABA and glutamate with MEGA-PRESS: reproducibility and gender effects. J Magn Reson Imaging. 33:1262–1267.

Pan JW, Avdievich N, Hetherington HP. 2010. J-refocused coherence transfer spectroscopic imaging at 7 T in human brain. Magn Reson Med. 64:1237–1246.

Popoli M, Yan Z, McEwen BS, Sanacora G. 2012. The stressed synapse: the impact of stress and glucocorticoids on glutamate transmission. Nat Rev Neurosci. 13:22–37.

Power JD, Barnes KA, Snyder AZ, Schlaggar BL, Petersen SE. 2012. Spurious but systematic correlations in functional connectivity MRI networks arise from subject motion. NeuroImage. 59:2142–2154.

Power JD, Barnes KA, Snyder AZ, Schlaggar BL, Petersen SE. 2013. Steps toward optimizing motion artifact removal in functional connectivity MRI; a reply to Carp. NeuroImage. 76:439–441.

Power JD, Mitra A, Laumann TO, Snyder AZ, Schlaggar BL, Petersen SE. 2014. Methods to detect, characterize, and remove motion artifact in resting state fMRI. NeuroImage. 84:320–341.

Power JD, Plitt M, Laumann TO, Martin A. 2017. Sources and implications of whole-brain fMRI signals in humans. NeuroImage. 146:609–625.

Power JD, Schlaggar BL, Petersen SE. 2015. Recent progress and outstanding issues in motion correction in resting state fMRI. NeuroImage. 105:536–551.

Prakash RS, Heo S, Voss MW, Patterson B, Kramer AF. 2012. Age-related differences in cortical recruitment and suppression: implications for cognitive performance. Behav Brain Res. 230:192–200.

Puts NA, Barker PB, Edden RA. 2013. Measuring the longitudinal relaxation time of GABA in vivo at 3 Tesla. J Magn Reson Imaging. 37:999–1003.

Qin P, Duncan N, Wiebking C, Gravel P, Lyttelton O, Hayes D, Verhaeghe J, Kostikov A, Schirrmacher R, Reader A, et al. 2012. GABAA receptors in visual and auditory cortex and neural activity changes during basic visual stimulation. Front Hum Neurosci. 6:337.

Rothman DL, Behar KL, Hetherington HP, Shulman RG. 1984. Homonuclear 1H double-resonance difference spectroscopy of the rat brain in vivo. Proc Natl Acad Sci USA. 81:6330–6334.

Rowland LM, Bustillo JR, Mullins PG, Jung RE, Lenroot R, Landgraf E, Barrow R, Yeo R, Lauriello J, Brooks WM. 2005. Effects of ketamine on anterior cingulate glutamate metabolism in healthy humans: a 4-T proton MRS study. Am J Psychiatry. 162:394–396.

Saad ZS, Gotts SJ, Murphy K, Chen G, Jo HJ, Martin A, Cox RW. 2012. Trouble at rest: how correlation patterns and group differences become distorted after global signal regression. Brain Connect. 2:25–32.

Sambataro F, Murty VP, Callicott JH, Tan HY, Das S, Weinberger DR, Mattay VS. 2010. Age-related alterations in default mode network: impact on working memory performance. Neurobiol Aging. 31:839–852.

Satterthwaite TD, Wolf DH, Loughead J, Ruparel K, Elliott MA, Hakonarson H, Gur RC, Gur RE. 2012. Impact of in-scanner head motion on multiple measures of functional connectivity: relevance for studies of neurodevelopment in youth. NeuroImage. 60:623–632.

Scheenen TW, Klomp DW, Wijnen JP, Heerschap A. 2008. Short echo time 1H-MRSI of the human brain at 3T with minimal chemical shift displacement errors using adiabatic refocusing pulses. Magn Reson Med. 59:1–6.

Siegel JS, Mitra A, Laumann TO, Seitzman BA, Raichle M, Corbetta M, Snyder AZ. 2017. Data quality influences observed links between functional connectivity and behavior. Cereb Cortex. 27:4492–4502.

Simpson R, Devenyi GA, Jezzard P, Hennessy TJ, Near J. 2017. Advanced processing and simulation of MRS data using the

FID appliance (FID-A) – an open source, MATLAB-based toolkit. Magn Reson Med. 77:23–33.

Singh KD, Fawcett IP. 2008. Transient and linearly graded deactivation of the human default-mode network by a visual detection task. NeuroImage. 41:100–112.

Srinivasan R, Cunningham C, Chen A, Vigneron D, Hurd R, Nelson S, Pelletier D. 2006. TE-averaged two-dimensional proton spectroscopic imaging of glutamate at 3T. NeuroImage. 30:1171–1178.

Stagg CJ, Bachtiar V, Johansen-Berg H. 2011. The role of GABA in human motor learning. Curr Biol. 21:480–484.

Sternberg S. 1966. High-speed scanning in human memory. Science. 153:652–654.

Terpstra M, Cheong I, Lyu T, Deelchand DK, Emir UE, Bednarik P, Eberly LE, Oz G. 2016. Test-retest reproducibility of neurochemical profiles with short-echo, single-voxel MR spectroscopy at 3T and 7T. Magn Reson Med. 76:1083–1091.

Terpstra M, Ugurbil K, Gruetter R. 2002. Direct in vivo measurement of human cerebral GABA concentration using MEGA-editing at 7 Tesla. Magn Reson Med. 47:1009–1012.

Tkac I, Starcuk Z, Choi IY, Gruetter R. 1999. In vivo H-1 NMR spectroscopy of rat brain at 1 ms echo time. Magnet Reson Med. 41:649–656.

Whitfield-Gabrieli S, Thermenos HW, Milanovic S, Tsuang MT, Faraone SV, McCarley RW, Shenton ME, Green AI, Nieto-Castanon A, LaViolette P, et al. 2009. Hyperactivity and hyperconnectivity of the default network in schizophrenia and in first-degree relatives of persons with schizophrenia. Proc Natl Acad Sci USA. 106:1279–1284.

Wiebking C, Duncan NW, Qin P, Hayes DJ, Lyttelton O, Gravel P, Verhaeghe J, Kostikov AP, Schirrmacher R, Reader AJ, et al. 2014a. External awareness and GABA – a multimodal imaging study combining fMRI and [18F]flumazenil-PET. Hum Brain Mapp. 35:173–184.

Wiebking C, Duncan NW, Tiret B, Hayes DJ, Marjanska M, Doyon J, Bajbouj M, Northoff G. 2014b. GABA in the insula – a predictor of the neural response to interoceptive awareness. NeuroImage. 86:10–18.

Xu S, Yang J, Li CQ, Zhu W, Shen J. 2005. Metabolic alterations in focally activated primary somatosensory cortex of alpha-chloralose-anesthetized rats measured by 1H MRS at 11.7T. NeuroImage. 28:401–409.

Yan CG, Cheung B, Kelly C, Colcombe S, Craddock RC, Di Martino A, Li Q, Zuo XN, Castellanos FX, Milham MP. 2013. A comprehensive assessment of regional variation in the impact of head micromovements on functional connectomics. NeuroImage. 76:183–201.

Yan CG, Zang YF. 2010. DPARSF: a MATLAB toolbox for "Pipeline" data analysis of resting-state fMRI. Front Syst Neurosci. 4:13.

Yizhar O, Fenno LE, Prigge M, Schneider F, Davidson TJ, O'Shea DJ, Sohal VS, Goshen I, Finkelstein J, Paz JT, et al. 2011. Neocortical excitation/inhibition balance in information processing and social dysfunction. Nature. 477: 171–178.

Zhu H, Edden RA, Ouwerkerk R, Barker PB. 2011. High resolution spectroscopic imaging of GABA at 3 Tesla. Magn Reson Med. 65:603–609.